Hindawi Publishing Corporation
Advances in Materials Science and Engineering
Volume 2016, Article ID 7645763, 10 pages
http://dx.doi.org/10.1155/2016/7645763

Research Article

Experimental Research on Hysteretic Characteristics of Steel Plates Artificially Corroded by Neutral Salt Spray

Shan-hua Xu, Guang-chong Qin, and Zong-xing Zhang

School of Civil Engineering, Xi'an University of Architecture and Technology, Xi'an, Shaanxi 710055, China

Correspondence should be addressed to Guang-chong Qin; qinguangchong@126.com

Received 9 November 2015; Revised 18 February 2016; Accepted 26 April 2016

Academic Editor: Seung-Jun Kwon

Copyright © 2016 Shan-hua Xu et al. This is an open access article distributed under the Creative Commons Attribution License, which permits unrestricted use, distribution, and reproduction in any medium, provided the original work is properly cited.

This paper aims to study the hysteretic characteristics of the steel plates artificially corroded by neutral salt spray. Salt spray was applied to accelerate the corrosion on the steel plates; specimens of varying degrees of corrosion were obtained in this manner. And each specimen was subject to cyclic loading test to get the hysteretic curve. Then the experimental results were extensively discussed, focusing on strength and ductility, hysteretic energy, the skeleton curve, and unloading and loading curve. After that, the hysteretic constitutive model of corroded steel was established based on the first time loading criterion, unloading criterion, cycle skeleton criterion, and reloading curve criterion. The result of the experiment showed that, with the increase of the degree of corrosion, the mechanical properties and seismic energy dissipation performance of seismic energy of the steel decreased; the deterioration of ductility got aggravated. On the other hand, the skeleton curve and the Ramberg-Osgood model were well matched, and the coefficient of circular enhancement showed a decreasing trend; the variation of cyclic hardening exponent did not have an obvious pattern. Meanwhile, the hysteretic constitutive model of corroded steel and the results of the experiment were well matched.

1. Introduction

Steel structure is widely used in large bridges, offshore oil platforms, industrial constructions, and residential buildings [1–3], as it has excellent mechanical properties and it is not expensive with good performance. Particularly its good ductility makes it easier to be the first choice for seismic design. However, if it is exposed to corrosive environment for a long time such as soil, air, acid rain, and seawater, it is easy to be corroded [4–7].

In order to study the phenomenon of the metal corrosion while being exposed in the real circumstance, some test methods are adopted to accelerate corrosion, such as exposing metal in hot and humid environment, using salt spray, using salt composite spray, and alternately exposing metal in wet and dry environments. Research had shown that [8–10] the accelerated corrosion test could represent the long-term natural exposure test. Moreover, it has shorter test cycle, and the test result can be reproduced. Nonetheless, it is difficult to simulate the natural environment completely due to the relatively big difference between the natural environment and the test conditions.

Corrosion will cause the mechanical properties of materials to degrade. Many scholars, who studied the deterioration of mechanical properties of corroded steel [11–15], had found that not only would the cross section of corroded steel reduce and the surface features change, but also the yield strength, the ultimate strength, and the ductility of corroded steel would reduce as well; and among them, the decrease of ductility was the most obvious one. In [16], author cut one corroded H shape steel and one noncorroded H shape steel which were actual engineering components and studied the hysteretic behaviors of bending under low cyclic loading. The results showed that the corroded specimen cracked faster than the noncorroded one, and the corroded specimen had fewer hysteretic cycles than the noncorroded one under the same loading system. In [17], the formulation and verification of a cyclic stress-strain relationship of reinforcing bars were presented. The cyclic loops followed Giuffré-Menegotto-Pinto [18] equations with some modifications to account for the effect of buckling. A complete path-dependent cyclic constitutive model was then obtained by combining the equations of the two monotonic envelopes and the cyclic

loops. Mendes and Castro [19] presented a new constitutive model for the simulation of reinforcing steel bars used in common reinforced concrete structures and it was designed to be used for general loading cases. The model included the well-known Guiffré-Menegotto-Pinto [18] softened branch, although new expressions were proposed for the evolutions of the curvature-related parameter and of the yield surface. Shi et al. [20] analyzed cyclic performance of high-strength structural steel and established an appropriate constitutive relationship. The study showed that the Q460D was similar to the ordinary strength steel [21] in some aspects, such as plasticity, cyclic hardening or softening, and Bauschinger effect [22]. Both experimental and modeling results showed that the responses of high-strength structural steel under cyclic loading and monotonic loading were different. The necking and fracture behavior would occur in advance for the former because the accumulated damage reduced the ductility of steel.

However, studying the damage accumulation of corroded steel and the cyclic plastic constitutive model of corroded steel under low cyclic loading are not covered in other researches. The hysteretic loop of steel under low cyclic loading belongs to low-cycle fatigue, and corrosion has a great and obvious effect on plastic deformation, crack growth, and fracture toughness of steel under low cyclic loading. Therefore, in order to study the hysteretic behaviors of the steel with different degrees of corrosion in the neutral salt spray environment and in order to study the cyclic plastic constitutive model, this paper will carry out the following experiment method. Firstly, the Q235 steel plate would undergo the process of accelerated corrosion. Secondly, cyclic loading tests would be carried out to analyze the hysteretic behavior of steel. Thirdly, the Ramberg-Osgood model [22] would be applied to compare the cyclic skeleton curves of steel in different corrosion conditions, and the corresponding parameters would be analyzed. Finally, a hysteretic constitutive model would be established, which could provide basic data for the study of the seismic behavior of steel structures.

2. Experimental Description

2.1. Corrosion Description. Neutral salt spray accelerated corrosion test was conducted to obtain the corroded specimens, based on the standard of GB/T 10125-2012 [23] and GB/T 24517-2009 [24], where chemical reagents (NaCl) and distilled water were adopted, the NaCl solution concentration was 50 mg/L, the pH value was 6.2–7.2, and the diameter of the nozzle and the rate of mist spray of the spraying equipment were 0.5 mm–1.5 mm and 0.5–1.5 L/(min·m^2), respectively. There were eight sets of specimens named A01–A71 (280 mm × 50 mm × 8 mm [25]). All specimens for corrosion were placed individually on an exposure test fixture which are parallel at an angle of 45° with regard to the vertical direction. The temperature and humidity were the same as the natural environment. In order to ensure the uniform corrosion of both sides of the test pieces, salt spray would be used on both sides of the test pieces every 2-3 days. All sample times (corrosion time): A11: 30 days, A21: 110 days, A31: 150 days, A41: 250 days, A51: 310 days, A61: 440 days. The specimens were retrieved and cleared away from the corrosion products with dilute hydrochloric acid and distilled water and then kept in CaO desiccator until the tensile test. In order to achieve the mass-loss rates of the corroded specimens, they were weighed with analytical balance before and after the accelerated corrosion test.

2.2. Cyclic Load Experiment. The specific sizes are shown in Figure 1(a). Loading device is the INSTRON Model 1343 which is a universal tension, compression, and torsion fatigue testing machine (Figure 1(c)). The displacement gauge distance was 50 mm, and its measuring range was 50% in the direction of tension and 10% in the pressure direction. The antibuckling device was designed to prevent the lateral buckling deformation of the plate under the action of larger pressure strain. The strain control was used to carry out large strain cyclic loading. Loading cycle was two times per level. Loading was applied with a 0.3% increase in amplitude. All of the cyclic loading waveforms were triangular wave and the strain loading rate was 0.00025/s. When the pressure strain reached 2.1%, the cyclic load was no longer applied, and then the specimen was subject to the uniaxial tensile load until the specimen cracked. The cyclic loading system is shown in Figure 1(b).

3. Experiment Result

3.1. Hysteretic Curve. It is difficult to measure the real strength of steel due to the uneven surface caused by corrosion. Therefore, the nominal stress (namely, the ratio of actual load to design area) was adopted to objectively reflect the effects of corrosion on the hysteretic behavior of steel. The hysteretic loading curves of all specimens are shown in Figure 2.

Figure 2 shows that steel hysteresis curves are divided into three parts including skeleton curve, unloading curve, and softening curve (reloading curve). The irregular changes in individual curves may be related to the antibuckling device and the displacement meter. The first loading curve of the steel extends along the monotonic curve, which is uniaxial tension effect. The unloading of the steel is in accordance with the elastic linear unloading, and the unloading stiffness is the same as that of the initial elastic modulus E_s, but with the increase of the strain, the elastic modulus of the unloading curve at all levels slightly decreases. The loading curve of the steel is the same as that of the loading curve of the same direction, which is in accordance with the model of the peak value. The peak stress of cyclic loading at the next stage of the steel has a greater dependence on the upper level. Steel was pulled into the plastic deformation stage, and stress is unloaded to zero. And then steel will undergo reverse loading to yield. The new yield stress decreases, which shows Bauschinger effect [22]. With the increase of strain, the stress of the steel increases, the effect of cyclic hardening occurs, and the strengthening effect of the steel is more obvious in the pulling direction than that in the pressing direction. Under the same strain amplitude, the hysteretic curves are

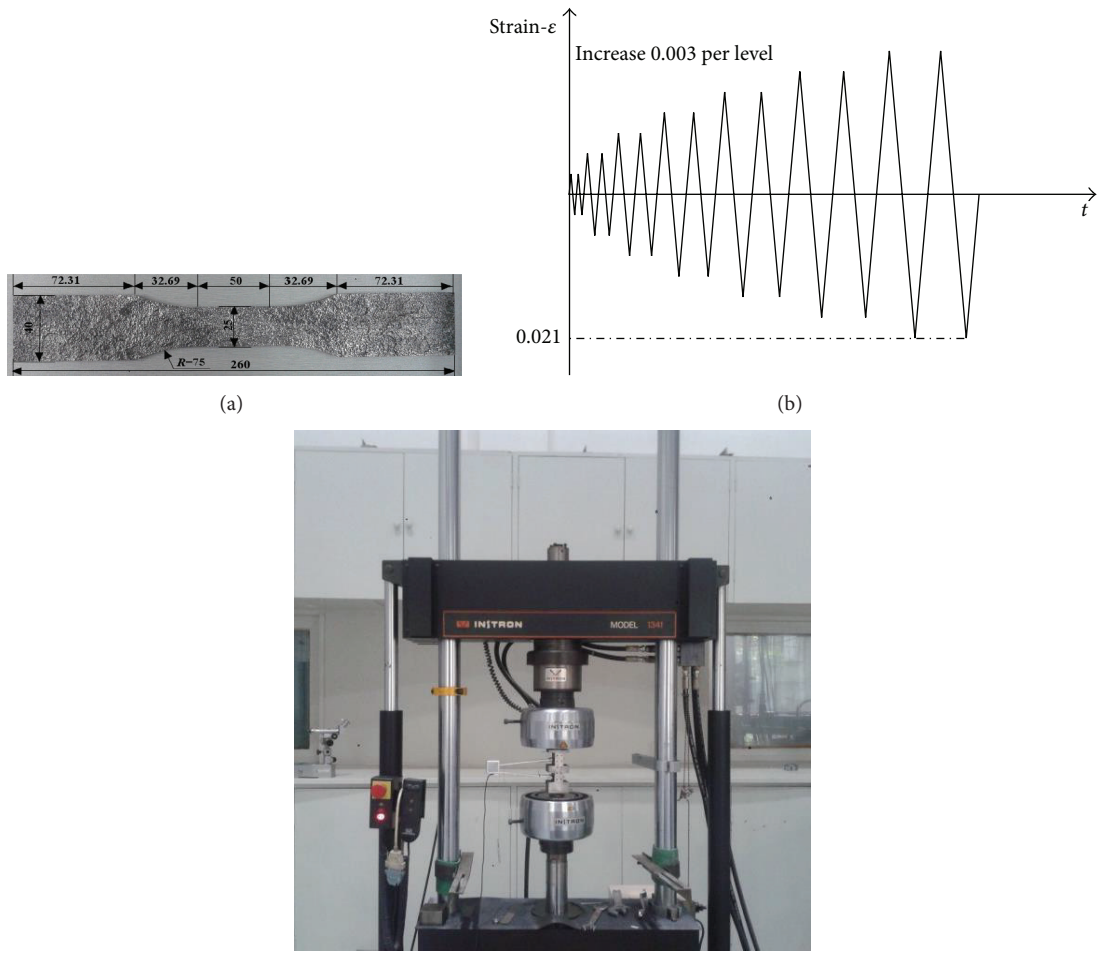

(a) (b) (c)

Figure 1: Size of experimental components, device, and system for loading.

not exactly the same as those in the target strain, and the stress in the last lap is greater than that in the previous lap. All hysteresis loops are plump, which shows that the corroded steel can also achieve full hysteresis loops, indicating seismic performance and energy dissipation capacity.

The difference between monotonic curve and hysteresis curve is shown in Figure 3. In cyclic loading scenario, the hardening or softening effect caused the change of stress-strain relationship until its stabilization. It shows that steel hysteresis and monotonic constitutive curves were quite different; for example, hardening phenomenon is quite obvious and the damage accumulation due to cyclic effect always leads the steel ductility to deteriorate, and the rate of stress decrease after peak point was significantly increased [21].

The main parameters of mechanical performance are shown in Table 1. The yielding effect of the steel under cyclic loading is not obvious, and so the corresponding strain of the steel is not listed. The ultimate strength is named f_u; the ultimate strain is named ε_u; and the breaking elongation is named δ. The hysteretic energy is obtained by calculating the area of the hysteresis loop. It reflects the seismic energy dissipation capacity of steel in the material level.

Table 1 shows that, with the increase of the degree of corrosion, the ultimate strength of steel under cyclic loading decreases. The strain corresponding to the ultimate strength and the elongation also shows a decreasing trend. During the process of the test, some of the corroded specimens cracked when they reached the maximum strength, which showed that the ductility of corroded steel was severely degraded under cyclic loading. The changes of hysteresis energy with different rates of weight loss are shown in Figure 4.

Compare the rate of corrosion with the hysteretic energy:

$$J = 64.499 \times \exp\left(-\frac{\rho_w}{13.541}\right) + 189.905, \quad (1)$$

where J is the hysteretic energy and ρ_w is the weight loss rate.

It can be seen that the dissipation performance of seismic energy decreases exponentially with the increase of the degree of corrosion under the same amount of cycles.

3.2. Skeleton Curve. The cyclic stress-strain skeleton curves of steel with different degrees of weight loss are shown in Figure 5. It can be seen that the steel has an obvious cyclic

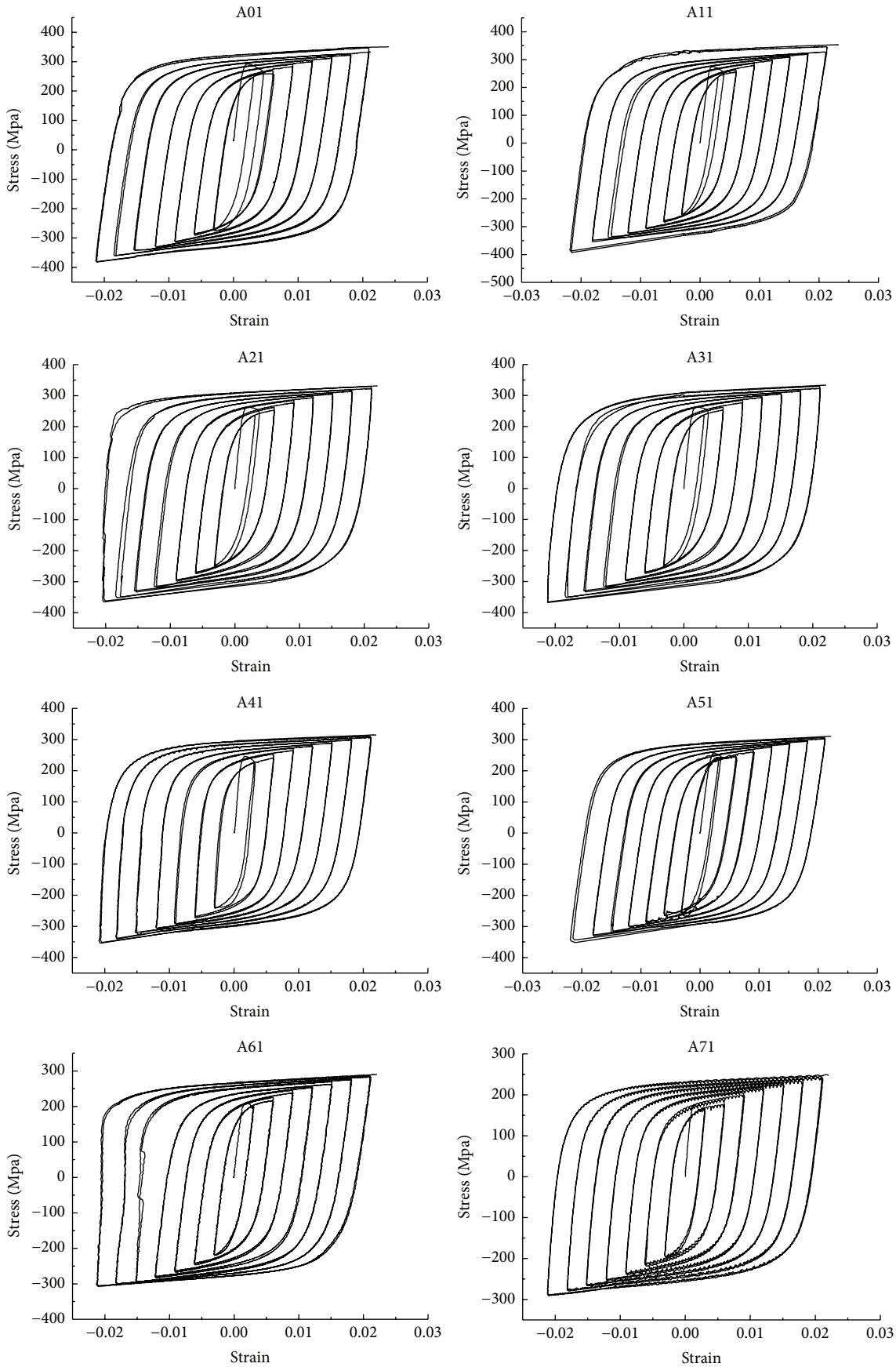

Figure 2: Hysteretic curve of specimen.

Table 1: Summary on mechanical properties of the specimen.

Serial number	Corrosion rate/%	f_u/MPa	ε_u	δ	Hysteresis laps	Hysteretic energy/MPa
A01	0	382.5	0.173	0.298	14	253.737
A11	5.08	374.75	0.171	0.278	14	236.679
A21	7.49	360	0.169	0.267	14	226.987
A31	7.89	364.75	0.167	0.265	14	226.391
A41	9.40	354.25	0.164	0.254	14	215.232
A51	10.47	356.95	0.166	0.256	14	225.762
A61	14.80	328.5	0.163	0.233	14	208.254
A71	18.82	306.85	0.149	0.208	14	207.808

Table 2: Skeleton curve model.

Number	A01	A11	A21	A31	A41	A51	A61	A71
E_s (10^5)/MPa	1.970	1.856	1.801	1.792	1.758	1.734	1.636	1.545
K'/MPa	816.813	626.500	592.927	584.254	551.420	567.530	545.944	534.919
n'	0.211	0.164	0.155	0.153	0.153	0.157	0.170	0.201

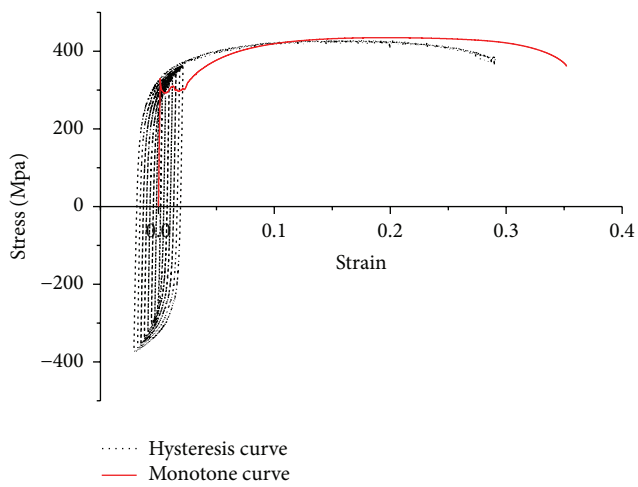

Figure 3: Comparison chart between monotonous and hysteresis curves.

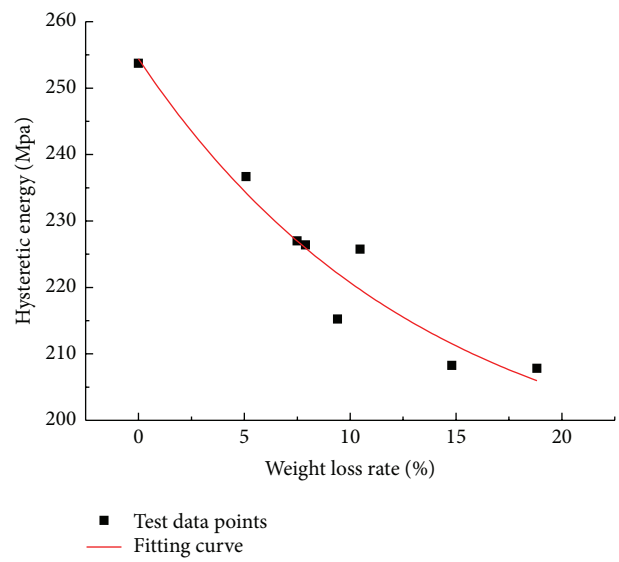

Figure 4: Hysteretic energy change with weight loss rate.

hardening behavior under cyclic loading but does not have a yield platform. Compared with the noncorroded steel, the strength of corroded steel appears to be lower. And the greater the degree of corrosion is, the more obvious the decrease of the strength becomes.

The maximum normal stress and normal strain obtained from the results of the experiment as well as the Ramberg-Osgood model [22] were used to be compared with the hysteretic skeleton curve of steel with different degrees of corrosion. Mathematical expressions of Ramberg-Osgood model [22] are as follows:

$$\frac{\Delta\varepsilon}{2} = \frac{\Delta\varepsilon_e}{2} + \frac{\Delta\varepsilon_p}{2} = \frac{\Delta\sigma}{2E_s} + \left(\frac{\Delta\sigma}{2K'}\right)^{1/n'}, \quad (2)$$

where $\Delta\varepsilon$ is the total strain amplitudes; $\Delta\varepsilon_e$ is the elastic strain amplitude; $\Delta\varepsilon_p$ is the shaping strain amplitude; E is the elastic modulus of steel; K' is the cyclic hardening coefficient; n' is the cyclic hardening index; $\Delta\sigma$ is the stable stress amplitude.

In order to make it easier to calculate and analyze, the mathematical expressions were simplified as follows:

$$\varepsilon = \frac{\sigma}{E_s} + \left(\frac{\sigma}{K'}\right)^{1/n'}. \quad (3)$$

Formula (3) was used to fit the cyclic loading skeleton curve. See Table 2 for the values of the cyclic hardening coefficient K' and of the cyclic hardening index n'. The fitting curve is shown in Figure 6. Figure 6 shows that Ramberg-Osgood model [22] fitted well with test data.

3.3. Parametric Degradation of Cyclic Skeleton Curve. Formula (3) shows that the right side of the model is composed of two parts. The first one shows the elastic characteristics of steel, which is linear expression; the second one shows the hardening effect of steel under cyclic loading, which is

Table 3: Cyclic hardening parameters.

Number	A01	A11	A21	A31	A41	A51	A61	A71
σ_y	236.451	222.67	216.132	215.046	210.950	208.048	179.942	154.496
a	541.571	381.042	358.927	349.929	348.703	345.251	311.33	306.544
b	−317.442	−171.496	−153.727	−148.409	−149.861	−149.231	−142.583	−159.821
c	−26.699	−56.401	−67.515	−74.386	−56.205	−64.317	−71.826	−44.761

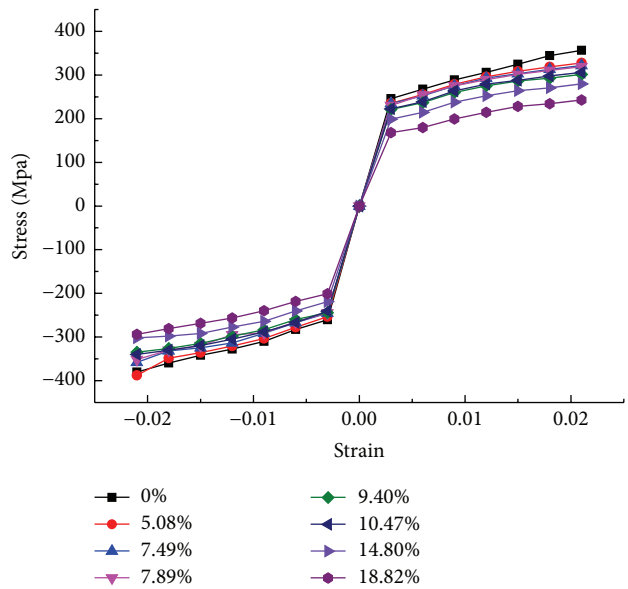

Figure 5: Hysteresis curve on varying degrees of corrosion steel.

exponential function. The cyclic hardening coefficient K' and the cyclic hardening exponent n' reflect the degree of the hardening of steel under cyclic loading [22].

The cyclic enhancement coefficient K' under different degrees of corrosion is shown in Figure 6. It can be seen that, with the increase of the rate of weight loss, the steel circulation strengthening coefficient decreases, whereas the variation of cyclic hardening exponent is small and does not have an obvious pattern. According to the definition of the exponential function, the decrease of the cyclic hardening coefficient indicates that, with the increasing degree of weight loss of the steel, the strengthening effect of the steel under cyclic loading is weakened. According to Figure 7, the relationship between the coefficient of cyclic hardening and the weight loss rate of steel plate is as follows:

$$K' = 85.926 \times \exp\left(-\frac{\rho_w}{0.046}\right) + 531.090. \quad (4)$$

The change of pattern of the cyclic hardening index n' is not obvious. The noncorroded steel plate is 0.211. The steel plate with corrosion rate of 19% is 0.201. When the weight loss rate is within 18%, the circular enhancement index n' is 0.16 n, in which the value of n can be 0.95–1.05.

4. Constitutive Model of Steel

Figure 2 shows that the hysteretic curve is mainly composed of three parts, the skeleton curve, the unloading curve, and the curve of the loading curve. The first loading curve of the steel extends along the monotonic curve, which is uniaxial tension effect. The unloading of the steel is in accordance with the elastic linear unloading, and the unloading stiffness is the same as that of the initial elastic modulus E_s. See Sections 2.2 and 3.1 for the first loading and the changes of the peak value of the steel. The unloading stiffness (initial elastic modulus E_s) is shown in Table 2.

4.1. Cyclic Skeleton Criterion. The Ramberg-Osgood model can relatively accurately simulate the shape of the circular skeleton curve; however, in this model, stress is the independent variable and strain is given as a function of stress, and it is difficult to obtain an explicit analytical expression of stress as a function of strain. This fact significantly increases calculation work when a strain value is given (e.g., measured from experiments) to initiate the program. According to [20, 21], and combining with the experimental data of this paper, a more efficient two-stage cyclic skeleton curve is proposed in the following and its performance is evaluated by the comparison with the experimental results in Figure 8. In the proposed curve, the first stage is elastic stage before yield and the second stage is the cyclic hardening stage, as given in

$$\sigma = \begin{cases} \sigma_y; & (\varepsilon \le \varepsilon_y) \\ a + b \times e^{(c \times \varepsilon)}; & (\varepsilon > \varepsilon_y). \end{cases} \quad (5)$$

In the formula, a, b, and c are used to control the shape of the circular skeleton curve. As the yield effect is not obvious under cyclic loading, the yield strength of the steel is not easy to determine. However, in the past researches on the behavior of the steel plate under monotonic tension, the corresponding strain values of the yield strength of the noncorroded steel plate and the corroded steel plate were all between 0.0013 and 0.0012. This paper took the stress which corresponded to the strain 0.0012 as the yield strength. Take A11 as an example. The comparisons of the tests and models are shown in Figure 8. It can be seen that the proposed form of function simulates the cyclic stress characteristics well under different rates of weight loss of Q235, which can reflect the curve of the circular skeleton.

Cyclic hardening parameters are shown in Table 3. According to the experimental data of corrosion rate and hysteresis curve, and the relationship between the parameters

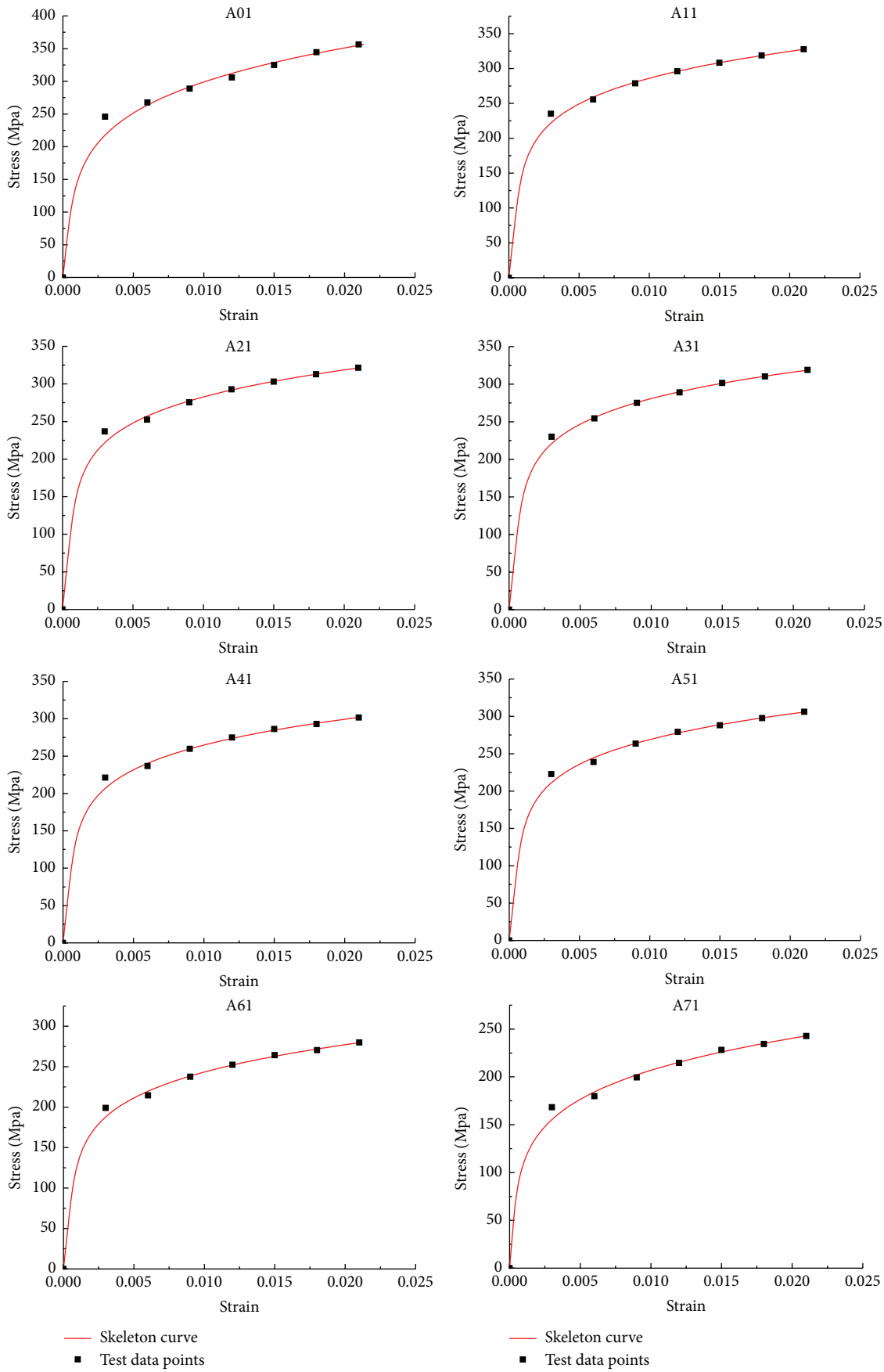

Figure 6: Fitting curve of skeleton model.

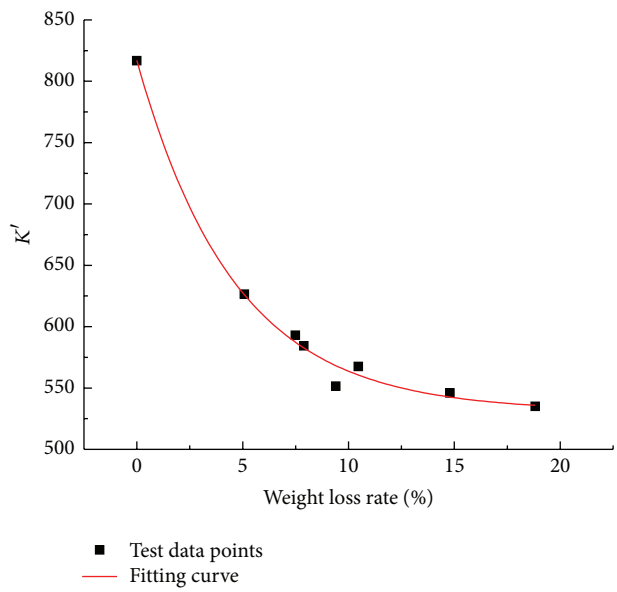

Figure 7: Relationship between recycling intensified factor and weight loss rate.

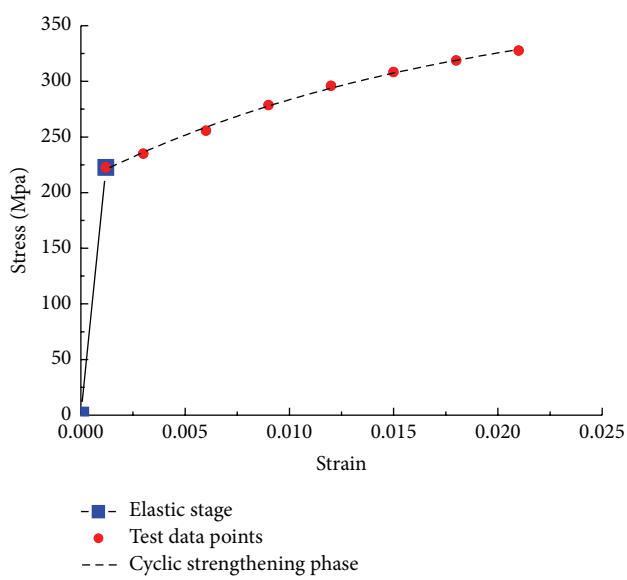

Figure 8: Model for skeleton curve of A11.

of the cyclic skeleton curve and the weight loss rate is shown in

$$\sigma_y = -23.898 \times \exp\left(-\frac{\rho_w}{-12.612}\right) + 260.006;$$
$$a = 234.421 \times \exp\left(-\frac{\rho_w}{4.961}\right) + 305.723; \quad (6)$$
$$b = -148.302 - 169.314 \times 0.651^{\rho_w}.$$

The pattern of the variation of coefficient C is not obvious. The value of coefficient C of the noncorrosive test pieces is −26.7. Under different rates of weight loss, the value of C is −62.2 K, and the K is within the range of 0.70–1.20.

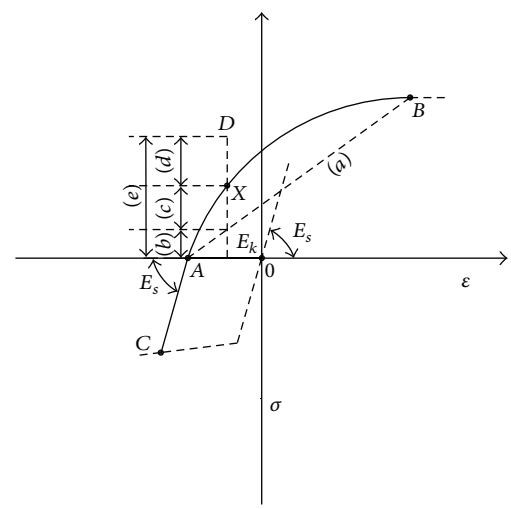

Figure 9: Reloading curve model.

4.2. Reload Criterion. Reloading curve mentioned in the calculation model [21] was applied and modified according to the results of the experiment, as shown in Figure 9.

As shown in Figure 9, the CA section is the unloading curve, and the AB section is the reloading curve for tension. The point A is the starting point of reloading curve $(\varepsilon_{Ai}, 0)$, and ε_{Ai} is defined as the corresponding values of displacement system; the point B is the target point of reloading curve for tension $(\varepsilon_{Bi}, \sigma_{Bi})$, defined as the maximum value for each cycle of the loop, referring to frame curve criterion; the point C is the target point of reloading curve for compression $(\varepsilon_{Bi}, \sigma_{Bi})$, defined as the maximum value for each cycle of the loop, referring to frame curve criterion; E_s is unloading slope (see Table 2); E_k is the angle between line a and ε axis. Assume that X point is required; then line b is $E_k(\varepsilon - \varepsilon_{Ai})$, line e is $E_s(\varepsilon - \varepsilon_{Ai})$, and line $c+d$ is $(E_s - E_k)(\varepsilon - \varepsilon_{Ai})$. Assume that the ratio of line d to line $c+d$ is η; then line d is $\eta(E_s - E_k)(\varepsilon - \varepsilon_{Ai})$.

The formula of stress and strain of X point is shown in

$$\sigma = E_s(\varepsilon - \varepsilon_A) + \sigma_A - (E_s - E_k)(\varepsilon - \varepsilon_A)\eta, \quad E_k = \frac{\sigma_B - \sigma_A}{\varepsilon_B - \varepsilon_A}, \quad (7)$$

where

$$\eta = a - \frac{b}{(\varepsilon - \varepsilon_A)/(\varepsilon_B - \varepsilon_A) + b}. \quad (8)$$

According to the results of the experiment, the coefficients a, b have no obvious patterns. The value of a is from 1.05 to 1.4, and the value of b is from 0.05 to 0.6.

4.3. Experiment and Model Comparison. According to the several criteria above and the results of the hysteretic curve test, the criterion of the development of hysteretic curve is shown in Figure 10. The target reaches the yield strength $A1$ when the curve is loaded on the 0-$A1$ curve for the first time (see Sections 2.2 and 3.1). According to the criterion of cyclic skeleton curves (see Section 3.1), it reaches $A2$. After reaching the unloading point of the steel, target will be unloaded from

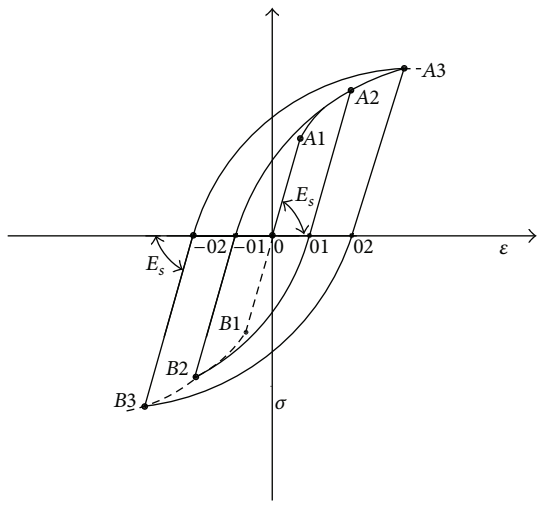

Figure 10: The specific description.

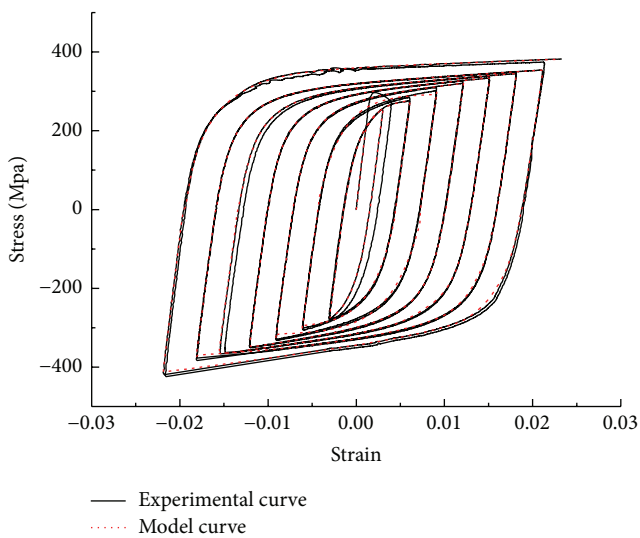

Figure 11: Comparison chart between model of the hysteresis criterion and experimental data of A11.

the elastic line to 01, assuming the unloading stiffness and the initial elastic modulus E_s are the same (see Table 2). Then the target reaches the peak value $B2$ in the first lap of the compression cycle (see Section 3.2). After being unloaded from the straight line, the target will reach −01. The unloading stiffness and the initial elastic modulus E_s are the same (see Table 2). After the target being pulled up to the maximum of $A2$, the second lap will start, and it will repeat the steps above (i.e., unloaded to 01, pressed to $B2$, and unloaded to −01). Finally the target will move along the reloading curve and pass through $A2$ to the unloading point $A3$ (see Sections 3.1 and 3.2); after elastic unloading, the target will reach the starting point of reloading curve for compression. Then the whole process above will be repeated.

By comparing the curve of cyclic constitutive model and hysteretic curve of steel plate under cyclic loading, A11, for example (Figure 11), had shown that the model matched the results of the experiment well. The steel loop constitutive model presented in this paper not only could predict the hysteretic behavior of the steel under different rates of weight loss but also could predict the residual strength of the specimen.

5. Conclusion

(1) Both noncorroded steel and corroded steel had shown behaviors like cyclic hardening, Bauschinger effect, and peak point effect under cyclic loading. The hysteresis loop was relatively plump. With the increase of the degree of weight loss, the mechanical properties of the steel were decreased, and the deterioration of ductility was aggravated.

(2) The Ramberg-Osgood model matched the skeleton curve of corroded steel under cyclic loading well. With the increase of the degree of weight loss, the coefficient of steel circular enhancement showed a decreasing trend, whereas the variation of cyclic hardening exponent was small and did not have an obvious pattern.

(3) In this paper, the hysteretic constitutional relationship of corroded steel was established based on the first time loading criterion, unloading criterion, cycle skeleton criterion, and reloading curve criterion. The model matched the results of the experiment well. Therefore, the steel loop constitutive model presented in this paper not only could predict the hysteretic behavior of steel under different rates of weight loss but also could predict the residual strength of the specimen.

Competing Interests

The authors declare that they have no competing interests.

Acknowledgments

The financial support is provided by the National Natural Science Foundation of China under Grant no. 51378417. This paper is also supported by Program for Changjiang Scholars and Innovative Research Team in University (IRT13089).

References

[1] ANSI/AISC, *Load and Resistance Factor Design Specification for Structural Steel Buildings*, American Institute of Steel Construction, Chicago, Ill, USA, 1999.

[2] V. Křivýa and P. Konečnýb, "Real material properties of weathering steels used in bridge structures," *Procedia Engineering*, vol. 57, pp. 624–633, 2013.

[3] S. Kravanja and T. Žula, "Cost optimization of industrial steel building structures," *Advances in Engineering Software*, vol. 41, no. 3, pp. 442–450, 2010.

[4] T. J. S. Yates, A. T. Coote, and R. N. Butlin, "The effect of acid deposition on buildings and building materials," *Construction and Building Materials*, vol. 2, no. 1, pp. 20–26, 1988.

[5] F. L. Laque, *Materine Corrosion Causes and Prevention*, John Wiley & Sons, New York, NY, USA, 1975.

[6] E. E. White and K. O. Watkins, "Design for prevention of corrosion in buildings and structures," *Corrosion*, vol. 9, no. 1, pp. 41–61, 1994.

[7] R. E. Melchers, "Effect of small compositional changes on marine immersion corrosion of low alloy steels," *Corrosion Science*, vol. 46, no. 7, pp. 1669–1691, 2004.

[8] R. E. Melchers, "Modeling of marine immersion corrosion for mild and low-alloy steels—part 1: phenomenological model," *Corrosion*, vol. 59, no. 4, pp. 319–334, 2003.

[9] R. E. Melchers and T. Wells, "Models for the anaerobic phases of marine immersion corrosion," *Corrosion Science*, vol. 48, no. 7, pp. 1791–1811, 2006.

[10] Z.-X. Wang, G.-A. Yu, and W. Han, "Investigation on interrelation of indoor accelerated corrosion and atmospheric exposure corrosion of steels," *Corrosion Science and Technology Protection*, vol. 16, no. 2, pp. 70–73, 2004.

[11] H. B. Li, Z. H. Jiang, H. Feng et al., "Microstructure, mechanical and corrosion properties of friction stir welded high nitrogen nickel-free austenitic stainless steel," *Materials & Design*, vol. 84, pp. 291–299, 2015.

[12] S. Sultana, Y. Wang, A. J. Sobey, J. A. Wharton, and R. A. Shenoi, "Influence of corrosion on the ultimate compressive strength of steel plates and stiffened panels," *Thin-Walled Structures*, vol. 96, pp. 95–104, 2015.

[13] Y. Wang, J. A. Wharton, and R. A. Shenoi, "Ultimate strength analysis of aged steel-plated structures exposed to marine corrosion damage: a review," *Corrosion Science*, vol. 86, pp. 42–60, 2014.

[14] M. R. Khedmati, M. M. Roshanali, and Z. H. M. E. Nouri, "Strength of steel plates with both-sides randomly distributed with corrosion wastage under uniaxial compression," *Thin-Walled Structures*, vol. 49, no. 2, pp. 325–342, 2011.

[15] S.-H. Xu and Y.-D. Wang, "Estimating the effects of corrosion pits on the fatigue life of steel plate based on the 3D profile," *International Journal of Fatigue*, vol. 72, pp. 27–41, 2015.

[16] M. Bruneau and S. M. Zahrai, "Effect of severe corrosion on cyclic ductility of steel," *Journal of Structural Engineering*, vol. 123, no. 11, pp. 1478–1486, 1997.

[17] R. P. Dhakal and K. Maekawa, "Path-dependent cyclic stress–strain relationship of reinforcing bar including buckling," *Engineering Structures*, vol. 24, no. 11, pp. 1383–1396, 2002.

[18] CEB, *RC Elements under Cyclic Loading: State of the Art Report*, Thomas Telford Services, London, UK, 1996.

[19] L. A. M. Mendes and L. M. S. S. Castro, "A simplified reinforcing steel model suitable for cyclic loading including ultra-low-cycle fatigue effects," *Engineering Structures*, vol. 68, pp. 155–164, 2014.

[20] G. Shi, M. Wang, Y. Bai, F. Wang, Y. Shi, and Y. Wang, "Experimental and modeling study of high-strength structural steel under cyclic loading," *Engineering Structures*, vol. 37, pp. 1–13, 2012.

[21] Y. J. Shi, M. Wang, and Y. Q. Wang, "Experimental and constitutive model study of structural steel under cyclic loading," *Journal of Constructional Steel Research*, vol. 67, no. 8, pp. 1185–1197, 2011.

[22] W. Ramberg and W. R. Osgood, "Description of stress-strain curves by three parameters," TN 902, National Advisory Committee for Aeronautics, 1943.

[23] GB/T 10125, *Corrosion Tests in Artificial Atmospheres-Salt Spray Tests*, Standards Press of China, Beijing, China, 2012 (Chinese).

[24] GB/T, "Corrosion of metals and alloys. Outdoors exposure test methods for periodic water spray," B/T 24517, Standards Press of China, Beijing, China, 2009 (Chinese).

[25] GB/T2975, *Steel and Steel Products-Location and Preparation of Test Pieces for Mechanical Testing*, Standards Press of China, Beijing, China, 1998 (Chinese).

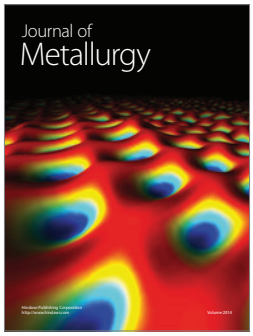

Hindawi

Submit your manuscripts at
http://www.hindawi.com